Measurement-Based Voltage Stability Assessment Considering Generator VAR Limits

Chengxi Liu, *Senior Member*, Fengkai Hu, Di Shi, *Senior Member*, *IEEE*, Xiaohu Zhang, *Member*, *IEEE*, Kai Sun, *Senior Member*, *IEEE*, Zhiwei Wang, *Member*, *IEEE*

***Abstract*—This paper proposes a measurement-based voltage stability assessment method considering VAR limits of generators. Traditional measurement-based methods for monitoring a load bus or a load area often simplify the external system as a simple constant electromotive force (e.m.f.) behind a Thevenin impedance, which may give inaccurate voltage stability margin when some external generator reaches its VAR limit. In this paper, a novel method is proposed to consider the VAR limits of generators by deriving a relationship between the variations of their e.m.f. and the load, which can be identified and tracked in real time. Thus, a more accurate voltage stability margin is derived by an analytical expression under variations of both generator terminal voltages and loads. The proposed method is compared with a typical Thevenin method and demonstrated on a two-area system and the IEEE 39-bus power system.**

***Index Terms*—Voltage stability assessment, Thevenin equivalent, generator capability, maximum power transfer, VAR limit.**

I. Introduction

DUE to fierce competitions in power markets, electric power grids are often operated close to their security limits, which significantly increases the risk of instabilities, e.g. voltage instability and angle instability [1], [2]. Voltage instability becomes one of the major concerns for system operators as it may propagate and induce cascading failures. Thus, it is of great importance to implement online Voltage Stability Assessment (VSA) to help system operators determine the voltage stability margin.

Traditionally, the VSA is performed with model-based approaches, such as Continuation Power Flow (CPF) or time-domain simulations [3]-[5]. Recently, the holomorphic embedding method is proposed to evaluate the voltage stability margin [6]-[9]. Several issues prevent the model-based approach from on-line applications, e.g., inaccurate models, possible divergence of state estimation and heavy computational burdens [1].

With wide deployment of the GPS-synchronized Phasor Measurement Units (PMUs), there are growing interests in the Measurement-Based VSA (MBVSA). One major category of MBVSA methods is based on Thevenin's theorem. Except for the load bus of interest, the rest of the system is reduced to its Thevenin Equivalent (TE) including a voltage source and an equivalent impedance, which are both estimated by local measurements [10]-[13]. A comparative study regarding four approaches to estimate the TE is provided in [14]. The authors in [15] derive a new TE circuit to consider the ZIP load model. Ref. [16]-[20] leverage the concepts of coupled single-port circuits or the channel component transformation to investigate the voltage stability issue for a load area. In [21], all the boundary buses within the load areas are merged together into a fictitious load bus, and then the TE is applied to this fictitious bus to evaluate the voltage stability margin for the load area. This method requires all boundary buses to be equipped with PMUs. Then, authors in [22] and [23] generalize the TE method to an N+1 bus equivalent system, where N is the number of boundary buses. Furthermore, ref. [24] extends the N+1 bus equivalent system to address potential N-1 contingencies in real time.

The existing TE-based approaches may perform well in predicting some of the Saddle Node Bifurcation (SNB) cases, but they are generally unable to predict the Limit Induced Bifurcation (LIB) due to the over-simplification of the external system. In practice, the LIB occurs often when generators or other voltage regulating devices reach their VAR limits while load continues to increase. Generators' reactive power capabilities play a crucial role in maintaining system voltage stability, as they can cause the system to lose its structural stability within a very short period, leading to voltage collapse [25], [26]. An MBVSA method capable of predicting both SNB and LIB is in great need.

Authors in [27] propose an alternative generator equivalent model considering VAR limits. The generators are modeled by time-varying internal voltages and impedances, whose parameters are estimated using the real-time measurements. Then, the L-index in [28] is extended on the model to give the voltage stability margin. Compared with the existing work, the proposed method in this paper can capture the relationship between the voltage and load when some generator hits its VAR limit. In addition, an analytical expression is derived to predict the voltage stability margin quickly and accurately.

This paper investigates the impacts of LIB in MBVSA and proposes a novel approach to incorporate generator VAR limits. Compared with existing approaches, the proposed one

This work is funded by SGCC Science and Technology Program, the ERC Program of the NSF and DOE under NSF grant *EEC-1041877*.

C. Liu is with the School of Electrical Engineering and Automation, Wuhan University, Wuhan, Hubei, 430072, China (Email: liuchengxi@whu.edu.cn).

F. Hu is with both GEIRI North America, San Jose, CA, USA, and the Department of EECS, the University of Tennessee, Knoxville, TN, USA (Email: fengkaihu@icloud.com).

D. Shi, X. Zhang, and Z. Wang are with GEIRI North America, 250 W. Tasman Dr., San Jose, CA, USA. (Email: di.shi@geirina.net; xiaohu.zhang@geirina.net; zhiwei.wang@geirina.net).

K. Sun is with the Department of Electrical Engineering and Computer Science, the University of Tennessee, Knoxville, TN, USA (Email: kaisun@utk.edu).

can provide system operators with more accurate stability margins and early warning of voltage instability by being able to handle both SNB and LIB.

The remainder of this paper is organized as follows. Section II presents the proposed solution and discusses its online implementation. Section III demonstrates the proposed approach on the two-area system and compares its performance against the existing TE-based method. Further experimental results are presented in Section IV, and conclusions are drawn in Section V.

II. Proposed Approach

A. Improved Generator Model for VSA

Power system voltage stability margin and its trajectory can vary significantly when one or more generators hit the VAR limits, as the incremental behavior(s) of that/those generator(s) will change dramatically. However, this effect is not considered in most of the existing TE-based approaches, which model the generator as a constant voltage source behand a Thevenin impedance. Considerable error in the estimation of system voltage stability margin has been observed using this type of simplified models.

The basic idea of the proposed method is to derive an approximate relationship on how the magnitude of the voltage source decreases with the increase of load after one or more generators reach VAR limits. Then, the voltage stability margin can be predicted in real time by evaluating an explicit expression considering VAR limits, so that the prediction of voltage stability margin can be more accurate. This method is used to prevent the mid-term or long-term voltage instability.

A decline in generator terminal voltage can be observed once the system enters LIB. To model and predict the variation of equivalent voltage source representing the external system, relation between the terminal voltage of this equivalent source and the load impedance can be derived by substituting the constant voltage source with a single-generator steady-state model as shown in Fig. 1.

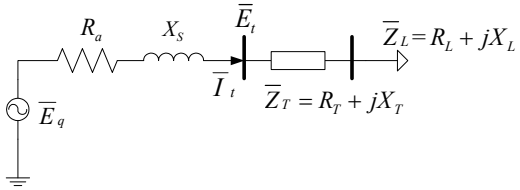

Fig. 1. Single-generator steady-state model for TE.

Neglecting the saliency, the armature terminal voltage $\bar{E}_t$ of a generator under a steady-state condition satisfies

$$\bar{E}_t = \bar{E}_q - (R_a + jX_s)\bar{I}_t \tag{1}$$

where $\bar{E}_q = jX_{ad}i_{fd}$ is an effective internal voltage representing the excitation voltage due to the field current. X_{ad} is the direct-axis mutual reactance. i_{fd} denotes the generator's field current. R_a and X_s are the armature resistance and synchronous reactance considering the flux produced by stator current [29].

Then the armature terminal current can be derived as

$$\bar{I}_t = \frac{\bar{E}_q - \bar{E}_t}{R_a + jX_s} \tag{2}$$

As shown in Fig. 1, the generator steady-state model is connected to a Thevenin impedance of the network, i.e. $\bar{Z}_T = R_T + jX_T$ and a load impedance, i.e. $\bar{Z}_L = R_L + jX_L$. Current $\bar{I}_t$ can also be calculated as

$$\bar{I}_t = \frac{\bar{E}_t}{\bar{Z}_T + \bar{Z}_L} \tag{3}$$

Combing (2) and (3) yields

$$\frac{\bar{E}_q - \bar{E}_t}{R_a + jX_s} = \frac{\bar{E}_t}{\bar{Z}_T + \bar{Z}_L} \tag{4}$$

Thus, the terminal voltage can be determined by

$$\bar{E}_t = \frac{jX_{ad}i_{fd}(\bar{Z}_T + \bar{Z}_L)}{R_a + jX_s + \bar{Z}_T + \bar{Z}_L} \tag{5}$$

where armature resistance R_a is typically very small and can be neglected. Equation (5) can be decomposed into the real part and imaginary part, expressed in (6) and (7) respectively.

$$E_{tR}\left(R_T + R_L\right) + X_{ad}i_{fd}\left(X_T + X_L\right) - E_{tI}\left(X_s + X_T + X_L\right) = 0 \tag{6}$$

$$E_{tR}\left(X_s + X_T + X_L\right) - X_{ad}i_{fd}\left(R_T + R_L\right) + E_{tI}\left(R_T + R_L\right) = 0 \tag{7}$$

where E_{tR} and E_{tI} are the real part and imaginary part of armature terminal voltage, i.e. $\bar{E}_t = E_{tR} + jE_{tI}$.

Eliminate the load reactance X_L in (6) and (7) to obtain

$$\left(\left|E_t\right|^2 + \left|E_q\right|^2\right)\left(R_T + R_L\right) = E_{tR}X_sX_{ad}i_{fd} + 2E_{tI}\left(R_T + R_L\right)X_{ad}i_{fd} \tag{8}$$

When the load keeps increasing, the equivalent load resistance R_L keeps decreasing. The terminal voltage $|E_t|$ keeps constant until the field current, i.e. i_{fd}, of a generator hits its maximum limit. After that, the terminal voltage $|E_t|$ decreases. The proposed model basically can predict the trend of E_t to give a more accurate margin after a generator hits its VAR limit.

When the single-generator model hits its VAR limit, the effective internal voltage $|E_q| = X_{ad}i_{fd}$ reaches its maximum. Rewrite (8) to obtain

$$X_{ad}^2 i_{fd}^2\left(R_T + R_L\right) - E_{tR}X_sX_{ad}i_{fd} = -\left(\left|E_t\right|^2 - 2E_{tI}X_{ad}i_{fd}\right)\left(R_T + R_L\right) \tag{9}$$

and set the error term as

$$\varepsilon = \left|E_t\right|^2 - 2E_{tI}X_{ad}i_{fd} \tag{10}$$

Therefore, the load resistance R_L can be determined by

$$R_L = \frac{E_{tR}X_sX_{ad}i_{fd}}{X_{ad}^2 i_{fd}^2 + \varepsilon} - R_T \tag{11}$$

Neglecting small error term ε, eq. (11) becomes

$$R_L \approx \frac{X_s}{X_{ad}i_{fd}}E_{tR} - R_T \tag{12}$$

Eq. (12) reveals an approximate linear relationship between the load resistance R_L and real part of generator terminal voltage E_{tR}. The error of this linear approximation is induced by in the error term ε in Eq. (11), which will be monitored later in the case studies.

In (12), the generator terminal voltage E_t is typically controlled by the Automatic Voltage Regulator (AVR) by adjusting the field current i_{fd}. E_t can be maintained at its reference value, until i_{fd} reaches its limit. With the linear approximation, coefficients $X_s/(X_{ad}i_{fd})$ and R_T in (12) can be estimated using E_{tR} and R_L measurements in a pre-defined time window. Therefore, the variation of generator terminal voltage

under heavy loading condition can be predicted, which can be more accurate than constant terminal voltage.

B. Network Transformation and Impact Factor

To generalize the single-generator model proposed in Section II-A, the multi-generator model shown in Fig. 2 can be regarded as an equivalent model representing many generators in a "source" area. Among these generators, the critical ones are the ones with higher impact factors than the others, which hold dominant components in the aggregated voltage source. With PMUs installed at these critical generators, the visibility of the system is largely improved, and the performance of generator over-excitation detection is further enhanced. Thus, the impact of critical generators to a power system can be assessed promptly utilizing the PMUs installed at these critical generators. To accurately address the impact factor and to create the equivalent coupled single-port model, the following network transformation is utilized.

In general, buses in an *M*-load *N*-generator power system can be categorized into three groups, namely, the load bus group **L**, the generator bus group **T**, and the bus group **Z** with zero current injection. Using the single-port decoupled method [18], power flow equations can be collectively written as

$$\begin{bmatrix} -\mathbf{I_L} \\ \mathbf{0} \\ \mathbf{I_T} \end{bmatrix} = \begin{bmatrix} \mathbf{Y_{LL}} & \mathbf{Y_{LZ}} & \mathbf{Y_{LT}} \\ \mathbf{Y_{ZL}} & \mathbf{Y_{ZZ}} & \mathbf{Y_{ZT}} \\ \mathbf{Y_{TL}} & \mathbf{Y_{TZ}} & \mathbf{Y_{TT}} \end{bmatrix} \begin{bmatrix} \mathbf{V_L} \\ \mathbf{V_Z} \\ \mathbf{E_T} \end{bmatrix} \tag{13}$$

where $-\mathbf{I_L}$ and $\mathbf{I_T}$ are vectors representing current injections at bus group **L** and **T**, respectively, and $\mathbf{V_L}$, $\mathbf{V_Z}$ and $\mathbf{E_T}$ represent the voltage phasors of the three groups. The system admittance matrix is rearranged accordingly as shown in (13).

The following transformation equation is proposed as

$$\mathbf{E}_{\text{eq}} = \mathbf{V_L} + \mathbf{Z}_{\text{eq}}\mathbf{I_L} \tag{14}$$

where the equivalent voltage source $\mathbf{E}_{\text{eq}}$ and impedance $\mathbf{Z}_{\text{eq}}$ of the single-port decoupled network are

$$\mathbf{Z}_{\text{eq}} = (\mathbf{Y_{LL}} - \mathbf{Y_{LZ}}\mathbf{Y_{ZZ}^{-1}}\mathbf{Y_{ZL}})^{-1} \tag{15}$$

$$\mathbf{E}_{\text{eq}} = \mathbf{Z}_{\text{eq}}(\mathbf{Y_{LZ}}\mathbf{Y_{ZZ}^{-1}}\mathbf{Y_{ZT}} - \mathbf{Y_{LT}})\mathbf{E_T} \tag{16}$$

Therefore, an impact factor matrix **K** can be defined as

$$\mathbf{K} = \mathbf{Z}_{\text{eq}}(\mathbf{Y_{LZ}}\mathbf{Y_{ZZ}^{-1}}\mathbf{Y_{ZT}} - \mathbf{Y_{LT}}) \tag{17}$$

In the following discussion, matrix **K** will be utilized to identify critical generators as well as to provide the ranking of generators in terms of their impacts in voltage stability monitoring and analysis.

Contingencies induced by switching actions can also be considered in the proposed method. In real-time operation, if there is an *N*-1 contingency, the admittance matrix in (13) will be updated, so a new voltage stability margin can be calculated using the updated matrix.

Fig. 2 shows a reduced power system model considering VAR limits of multiple generators. For example, a load $\bar{Z}_{L1}$ is connected to *N* generators through multiple equivalent transmission lines with impedances, $\bar{Z}_{T11}$- $\bar{Z}_{TN1}$, which are defined in the 1st column of matrix $\mathbf{Z}_{\text{eq}}$. Fig. 3 shows the single-port equivalent model considering VAR limits after the network transformation in (15)-(17).

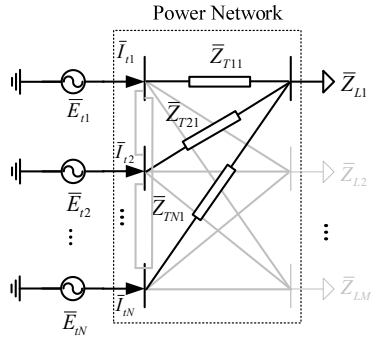

Fig. 2. Power system equivalent considering generator VAR limits.

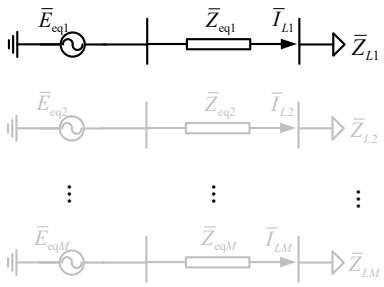

Fig. 3. Single-port equivalent model considering generator VAR limits.

Representing matrix **K** with $\bar{K}_{ij}$ ($1 \le i \le M$, $1 \le j \le N$), Eq. (17) can be rewritten as

$$\mathbf{E}_{\text{eq}} = \begin{bmatrix} \bar{K}_{11} & \bar{K}_{12} & \cdots & \bar{K}_{1N} \\ \bar{K}_{21} & \bar{K}_{22} & \cdots & \bar{K}_{2N} \\ \vdots & \vdots & \ddots & \vdots \\ \bar{K}_{M1} & \bar{K}_{M2} & \cdots & \bar{K}_{MN} \end{bmatrix} \begin{bmatrix} \bar{E}_{t1} \\ \bar{E}_{t2} \\ \vdots \\ \bar{E}_{tN} \end{bmatrix} \tag{18}$$

$$\bar{E}_{\text{eq}i} = \sum_{j=1}^{N} \bar{K}_{ij}\bar{E}_{tj} = \bar{K}_{i1}\bar{E}_{t1} + \bar{K}_{i2}\bar{E}_{t2} + \cdots + \bar{K}_{iN}\bar{E}_{tN} \tag{19}$$

which reveals the relationship between an equivalent voltage source $\bar{E}_{\text{eq}}$ and a generator terminal voltage $\bar{E}_t$. The element K_{ij} in matrix **K** indicates the level of impact of the j^{th} generator on the i^{th} load.

For a specific load bus, the load increase would have the main impacts on some of its adjacent generators. For different load buses, the critical generators can be different, which are identified from the ones with the largest K_{ij} in the i^{th} row of the matrix **K**.

As shown in (12), under specific conditions, a linear relationship between a generator terminal voltage E_{tR} and load resistance R_L has been derived. To generalize this observation, one possible scenario under consideration is that multiple generators hit their VAR limits at different time instants, each with a different E_{tR}-R_L curve. In this case, voltage magnitude E_{tR} is piece-wise linear with respect to R_L. To describe this relationship, multiple estimates for E_{tR} are needed. The least squares approach in [10] can be adopted to estimate E_{tR} and Z_T over a sliding time window. Note that there are 4 real unknowns to solve, i.e.:

$$\begin{bmatrix} E_{tR} & E_{tI} & R_T & X_T \end{bmatrix} = (\mathbf{H}^{\mathbf{T}}\mathbf{H})^{-1}\mathbf{H}^{\mathbf{T}}\mathbf{Z} \tag{20}$$

$$\mathbf{H} = \begin{bmatrix} V_{R,1} & V_{I,1} & -p_1 & -q_1 \\ V_{I,1} & -V_{R,1} & -q_1 & p_1 \\ \vdots & \vdots & \vdots & \vdots \\ V_{R,n} & V_{I,n} & -p_n & -q_n \\ V_{I,n} & -V_{R,n} & -q_n & p_n \end{bmatrix} \tag{21}$$

$$\mathbf{Z}^{\mathrm{T}} = \begin{bmatrix} V_{R,1}^2+V_{I,1}^2 & 0 & V_{R,n}^2+V_{I,n}^2 & 0 \end{bmatrix} \tag{22}$$

where $\bar{E}_t = E_{tR} + jE_{tI}$, $\bar{Z}_T = R_T + jX_T$, and matrices **H** and **Z** are calculated based on PMU measurements collected at n time instants within the specified time window. Variables $V_{R,k}$ and $V_{I,k}$ are real and imaginary parts of voltage at the load bus at the k^{th} time step, respectively. Variables p_k and q_k are active and reactive power injections at the load bus at the k^{th} time step. As mentioned before, this method is used to prevent the mid-term or long-term voltage instability, so $\bar{E}_t$ and $\bar{Z}_T$ are assumed to be constant in the time windows of parameter identification.

With at least two sets of Thevenin equivalent parameters obtained, least squares approach can be used to identify coefficients a and b as shown below to model the linear relationship between E_{tR} and R_L:

$$E_{tR} = \frac{X_{ad} i_{fd}}{X_s} R_L + \frac{X_{ad} i_{fd} R_T}{X_s} + \varepsilon' = aR_L + b + \varepsilon' \tag{23}$$

where ε' is the derived error term, i.e. $\varepsilon' = \varepsilon(R_T+R_L)X_s X_{fd} i_{fd}$, in which ε is the error term in Eq. (10). ε' will be monitored later in the case studies.

C. Voltage Stability Limit Calculation

With generators' reactive power capabilities considered, more accurate voltage stability limits can be evaluated with prediction of E_t, which is discussed in this subsection. As mentioned in the previous subsection, the real part of each terminal voltage E_{tR} varies linearly with the i^{th} load resistance R_L, and the equivalent voltage source E_{eq} for this load is the linear combination of all terminal voltages E_{tj} (j=1-N), according to (19). The following derivation proves that the real and imaginary parts of equivalent voltage source E_{eq} of single-port equivalent model also have the linear relationship with the load resistance R_L, expressed as

$$\begin{aligned} E_{\text{eq}R} &= \mathrm{Re}\left(\sum_{j=1}^{N} \bar{K}_{ij} \bar{E}_{tj} \right) \\ &= \sum_{j=1}^{N} \mathrm{Re}\left(\bar{K}_{ij}\right)\left(a_j R_L + b_j\right) - \sum_{j=1}^{N} \mathrm{Im}\left(\bar{K}_{ij}\right) E_{tIj} = a'R_L + b' \\ E_{\text{eq}I} &= \mathrm{Im}\left(\sum_{j=1}^{N} \bar{K}_{ij} \bar{E}_{tj} \right) \\ &= \sum_{j=1}^{N} \mathrm{Im}\left(\bar{K}_{ij}\right)\left(a_j R_L + b_j\right) + \sum_{j=1}^{N} \mathrm{Re}\left(\bar{K}_{ij}\right) E_{tIj} = a''R_L + b'' \end{aligned} \tag{24}$$

where a_j, b_j are the linear coefficient of the j^{th} generator and a', b', a'' and b'' are parameters, such that

$$\begin{aligned} a' &= \sum_{j=1}^{N} a_j \,\mathrm{Re}\left(\bar{K}_{ij}\right), \quad b' = \sum_{j=1}^{N} \left[b_j \,\mathrm{Re}\left(\bar{K}_{ij}\right) - \mathrm{Im}\left(\bar{K}_{ij}\right) E_{tIj} \right] \\ a'' &= \sum_{j=1}^{N} a_j \,\mathrm{Im}\left(\bar{K}_{ij}\right), \quad b'' = \sum_{j=1}^{N} \left[b_j \,\mathrm{Im}\left(\bar{K}_{ij}\right) + \mathrm{Re}\left(\bar{K}_{ij}\right) E_{tIj} \right] \end{aligned} \tag{25}$$

For the single-port model, shown in Fig. 3, assuming the impedance of a critical load is represented as $\bar{Z}_L$, its power consumption can be calculated as

$$\bar{S}_L = \bar{V}_L \bar{I}_L^{\,*} = P_L + jQ_L \tag{26}$$

$$P_L = \frac{R_L \left|E_{eq}\right|^2}{(R_{\text{eq}}+R_L)^2 + (X_{\text{eq}}+X_L)^2} = \frac{R_L\left[\left(a'R_L+b'\right)^2 + \left(a''R_L+b''\right)^2\right]}{(R_{\text{eq}}+R_L)^2 + (X_{\text{eq}}+X_L)^2} \tag{27}$$

$$Q_L = \frac{X_L \left|E_{eq}\right|^2}{(R_{\text{eq}}+R_L)^2 + (X_{\text{eq}}+X_L)^2} = \frac{X_L\left[\left(a'R_L+b'\right)^2 + \left(a''R_L+b''\right)^2\right]}{(R_{\text{eq}}+R_L)^2 + (X_{\text{eq}}+X_L)^2} \tag{28}$$

where R_L and X_L are resistance and reactance of the load.

A linear or quadratic function can be utilized to represent the load impedance characteristic. To simplify the mathematical derivation, an assumption can be made that the load reactance is proportional to its resistance as:

$$\gamma = \frac{X_L}{R_L} \tag{29}$$

Thus, by taking derivative of (27) with respect to load resistance, the 'nose' point can be calculated.

$$\frac{dP_L}{dR_L} = 0 \tag{30}$$

Solve (30) to obtain the following equations:

$$\left(cR_L + d\right) f(R_L) = 0 \tag{31}$$

where parameters

$$c = 2\left(a'^2 + a''^2\right) \tag{32}$$

$$d = 2\left(a'b' + a''b''\right) \tag{33}$$

and

$$\begin{aligned} f(R_L) = c\left(\gamma^2+1\right)R_L^3 + \left[4c\left(R_T+\gamma X_T\right) - d\left(\gamma^2+1\right)\right]R_L^2 + \\ 3c\left(R_T^2+X_T^2\right)R_L + d\left(R_T^2+X_T^2\right) \end{aligned} \tag{34}$$

Obviously, $-d/c$ is one of the roots of the 4$^{\text{th}}$ order polynomial equation regarding R_L in (31). According to (23), both c and d are positive real numbers. Therefore, this root is practically infeasible and can be neglected as R_L cannot be negative.

The roots exist in the following cubic equation.

$$\begin{aligned} c\left(\gamma^2+1\right)R_L^3 + \left[4c\left(R_T+\gamma X_T\right) - d\left(\gamma^2+1\right)\right]R_L^2 + \\ 3c\left(R_T^2+X_T^2\right)R_L + d\left(R_T^2+X_T^2\right) = 0 \end{aligned} \tag{35}$$

Since all coefficients in this cubic equation are real, there exists at least one real root. All remaining roots of this cubic equation can be found algebraically, as shown in (36). The maximum power that can be supplied to the load is shown in (41).

$$R_{L,m}=-\frac{1}{3c\left(\gamma^2+1\right)}\begin{pmatrix}4c\left(R_T+\gamma X_T\right)-d\left(\gamma^2+1\right)+\\ \left(-\frac{1}{2}+\frac{1}{2}\sqrt{3}i\right)^m C+\\ \Delta_0\left(-\frac{1}{2}+\frac{1}{2}\sqrt{3}i\right)^{-m} C^{-1}\end{pmatrix},m\in\{0,1,2\} \tag{36}$$

$$C=\sqrt[3]{\frac{\Delta_1\pm\sqrt{\Delta_1^2-4\Delta_0^3}}{2}} \tag{37}$$

$$\Delta_0=D^2-9c^2\left(\gamma^2+1\right)\left(R_T^2+X_T^2\right) \tag{38}$$

$$\Delta_1=27c^2\left(\gamma^2+1\right)\left(R_T^2+X_T^2\right)\left[D+d\left(\gamma^2+1\right)\right]-2D^3 \tag{39}$$

$$D=d\gamma^2-4c\gamma X_T+d-4cR_T \tag{40}$$

$$P_{\max}=\max_{m\in\{0,1,2\}}\left\{\frac{R_{L,m}\left[\left(a'R_L+b'\right)^2+\left(a''R_L+b''\right)^2\right]}{\left(R_T+R_{L,m}\right)^2+\left(X_T+\gamma R_{L,m}\right)^2}\right\} \tag{41}$$

D. Scheme for Online Implementation

A flow chart of the proposed approach is shown in Fig. 4. As discussed in the previous subsections, the maximum active power transfer limit can be evaluated numerically. According to (41), to track this limit in real time, parameters $R_{L,m}$ in (36) need to be estimated and updated promptly on a regular basis, which requires real-time parameter identification of the equivalent voltage source and the Thevenin equivalent.

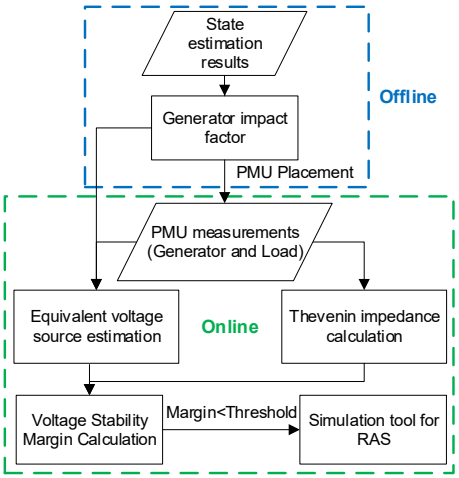

Fig. 4. Flowchart of the proposed method.

Admittances in the power flow data obtained from state estimation can be used to calculate generator impact factors, which serve as initial estimates of equivalent voltage source. Toward this end, PMU measurements at critical generator buses are needed to estimate parameters of the equivalent voltage source and Thevenin impedance. Determination of these critical generators is based on the ranking of the impact factors. In practice, the impact factors of all generators for the entire power system under investigation are calculated offline, and the ranking of these impact factors indicates a sequential PMU placement strategy. This sequential strategy endows MBVSA method with the scalability regarding the availability of measurements. PMU measurements from load buses also need to be collected in order to evaluate active and reactive power consumptions which ultimately are used for the voltage stability margin calculation. This stability margin information will be provided to operators and the simulation tools for remedial action scheme (RAS). When the real-time stability margin is smaller than a pre-defined threshold, the commercial software for model-based VSA will be called to conduct power flow calculations or dynamic simulations for multiple contingencies. Additionally, the RAS actions will also be validated.

It is worthwhile to mention that P_{max} is calculated by Eq. (41) in an analytical manner, which is fast to be evaluated in real time. Meanwhile, P_{max} can be calculated with higher accuracy when some generators hit the VAR limits, because it considers the additional information of the linear approximation between the variations of voltage sources and the increase of load.

This MBVSA method is able to predict voltage stability limit, i.e. P_{max}, considering both SNB and LIB. When one or more generators hit their VAR limits, their over excitation limit (OEL) alarm signals will be transmitted to the EMS system in the control center. If there is no OEL alarm activated, i.e. SNB, the voltage stability margin will be calculated by the method in [23] without considering VAR limits. If some OEL alarms are activated in generators, i.e. LIB, the margin will adapt to the proposed method. It can give a more accurate stability margin with considering the trend of E_t for those generators working under VAR limits.

Contingencies induced by switching actions can also be considered in the proposed method. If there is an N-1 contingency, the admittance matrix in (13) will be updated in real time, so a new voltage stability margin can be calculated using the updated matrix.

III. Demonstration on the Two-area System

The two-area system given by P. Kundur [29] is used to demonstrate the proposed approach. Fig. 5 shows a one-line diagram of this two-area system, a circuit model of which is built and simulated using MATLAB. In this circuit model, all the generators are represented as voltage sources, where the voltage magnitude of generator G4 is declining to emulate the scenario when VAR limit of generator G4 is reached. The load at Bus 9 is increased from 1767 MW to 2665 MW, with voltage collapse observed at the end of the simulation.

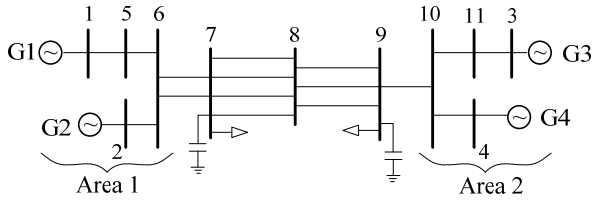

Fig. 5. The two-area system.

Fig. 6(a) shows the PV curve of Bus 9, from which it can be seen that the "nose" point is at 0.72 p.u. when load at Bus 9 reaches 2665 MW. Fig. 6(b) shows the impact factors of all four generators, they are calculated using the system

admittance matrix. Basically, generator G4 at Bus 4 has the largest impact factor which is greater than the summation of the impact factors of the rest three, and therefore is considered as the critical generator.

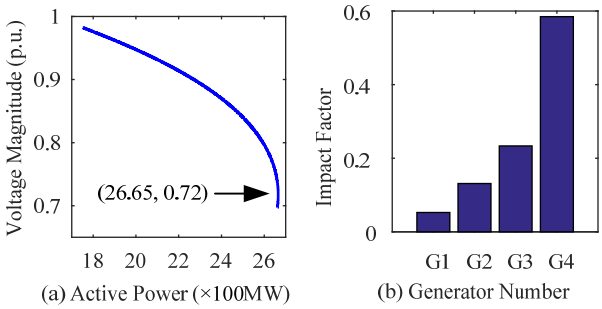

Fig. 6. (a) PV curve of bus 9 and (b) Impact factor of the generators.

Assume PMUs are deployed at all critical generators and Load 9 in the system. They are monitoring the voltage phasors of the generators and Load 9, which are utilized to calculate the coefficients a and b in (23). This equation is solved by least squares approach showing in (20)-(22). With such a linear relation estimated, the equivalent voltage source $\overline{E}_{qi}$ can be obtained using (19). Finally, the voltage stability can be calculated according Section II-C.

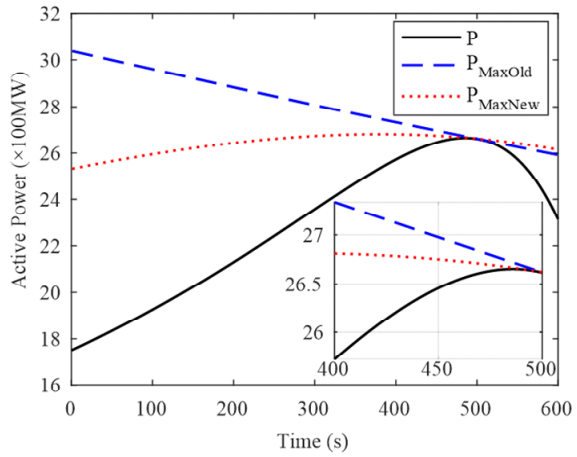

Fig. 7. Pmax comparison.

Fig. 7 shows the active power transfer (black line) and its corresponding limits calculated using both classical TE-based method [1] (blue line) and the proposed method (red line). As the figure shows, the proposed method always provides more accurate result for the active power limit calculation, since P_{MaxNew} estimated by the new method is closer to the actual P_{Max} = 2665MW, which is identified by time domain simulation, and more flat than P_{MaxOld} which is calculated by the TE based method. The classical TE-based method gives a wrong positive margin when the load reaches its 'nose' point with zero margin, while the proposed approach can identify it more accurately.

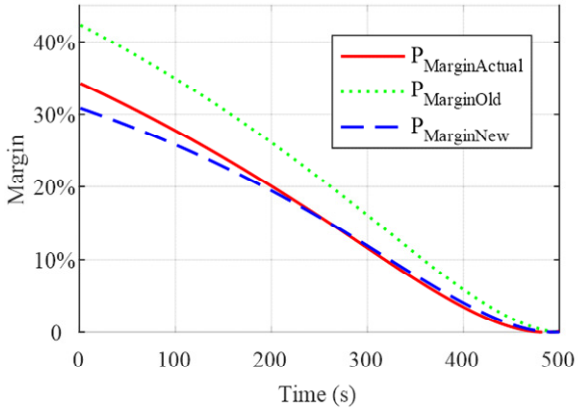

Fig. 8. Comparison of P margins.

Comparison of the active power transfer margins is plotted in Fig. 8. These margins are calculated as the differences between the calculated (actual) maximum power transfer limit and the actual power transfer divided by the corresponding maximum power transfer limit. At t = 0s, errors in the transfer margin calculation are 3.45% and 8.07% using the proposed approach and the classical TE approach, respectively. As load increases, estimation error associated with the proposed method drops significantly and gets close to zero after 200s. However, the error resulting from classical TE-based method is always significantly higher. Therefore, the effectiveness and advantage of the proposed approach have been demonstrated by the two-area system.

IV. Case Studies on the IEEE 39-Bus System

The proposed method is further tested on the IEEE New England 39-bus system. As highlighted in Fig. 9, the system has a Connecticut Load Center (CLC) area supported by power from three tie lines, i.e., Line 9-8, 3-4, and 15-14. Line 9-8 is from the NYISO region and the other two are from the northern ISO-NE region.

Fig. 9. Map of IEEE 39 system.

DSA*Tools*™ is used to simulate the voltage instability scenario. In the simulation, all loads are modeled as constant PQ loads. Simulation results on the voltages and the complex

powers at Bus 8 are recorded at 30Hz. The proposed method is performed every 1/30s using data collected from the latest 1s time window.

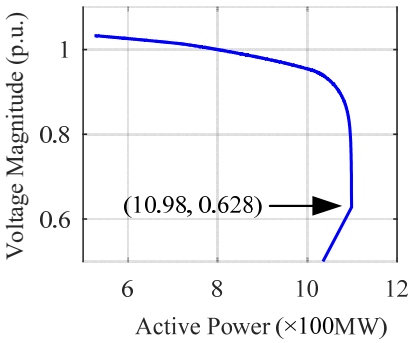

Fig. 10. PV curve of Bus 8.

To simulate the voltage collapse in the CLC area, load at Bus 8 is continuously increased by a total of 576 MW from its original loading level of 522 MW with consistent load power factor. Fig. 10 shows the PV curve at Bus 8. The voltage collapse happens around t = 173s as shown in Fig. 11.

The generator terminal voltage magnitudes recorded throughout this simulation are plotted in Fig. 11. The black curve V_{mE} represents voltage at the aggregated bus for Load 8. Three stages with different slopes can be observed on V_{mE}, which are in [0s, 60s], [60s, 150s] and [150s, 173s], respectively. The stage shift at 60s is caused by the over-excitation of generator G31, and the stage change at 150s is caused by the over-excitation of generator G32. The voltages at Bus 31 and Bus 32 start dropping significantly after 60s and 150s, respectively.

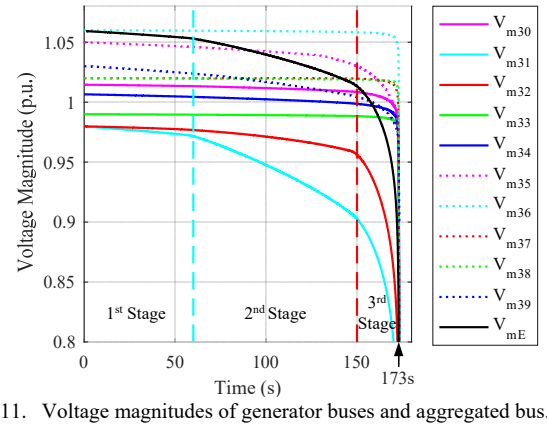

Fig. 11. Voltage magnitudes of generator buses and aggregated bus.

According to (17) , generator impact factors are calculated and shown in Fig. 12. Generators G31, G32 and G39 have the highest impact factors. As shown in the geographic map (Fig. 9), these three generators are the nearest ones to Load 8. Therefore, both the electrical distance and geographic information tell the same story for the critical generators.

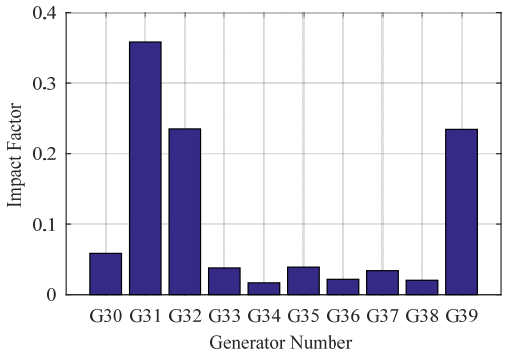

Fig. 12. Generator impact factor.

With the impact factors calculated, the equivalent voltage source can be estimated according to (19). In practice, the equivalent voltage source is updated continually in real time using the PMU measurements from all the generator buses. Additionally, Load 9 is monitored by PMU, which helps identifying the coefficients in (23). At the end, the voltage stability limit can be solved in real time by (36)-(41).

To further verify the aggregation results, the correlation coefficient is also used to measure the linear dependence between the voltage profiles at the aggregated bus and the corresponding original ones. If there are N measurements in each voltage profile, the Pearson correlation coefficient is evaluated as

$$\rho(V_{mi},V_{mE}) = \frac{\mathrm{cov}(V_{mi},V_{mE})}{\sigma_{V_{mi}}\sigma_{V_{mE}}} = \frac{1}{N-1}\sum_{j=n}^{N}\left(\frac{\overline{V_{mi}(j)}-\mu_{V_{mi}}}{\sigma_{V_{mi}}}\right)\left(\frac{V_{mE}(j)-\mu_{V_{mE}}}{\sigma_{V_{mE}}}\right) \quad (42)$$

where μ_{Vmi} and σ_{Vmi} are the mean and standard deviation of V_{mi} (i=30-39), respectively, and μ_{VmE} and σ_{VmE} are the mean and standard deviation of voltage V_{mE} at the aggregated bus. As shown in Fig. 13, the correlation coefficients for each generator terminal voltage magnitude and the equivalent voltage magnitude are calculated, among which the top three are the ones between V_{m31}, V_{m32} and V_{m35}.

By comparing the actual point of operation to the desired limit, the regulator determines when it is appropriate to adjust the generator field current in order to stay within the desired operating conditions. Fig. 14 shows the field currents for all ten generators in the system. The three solid curves reaching their limits sequentially are the field currents of generators G31, G32 and G35. The field current of generator G31 firstly reaches the limit at 60s, then field current of generator G35 hits its limit at 130s, and finally field current of generator G32 reaches its limit at 150s. The remaining generators do not hit their field current limits, and therefore their field currents keep increasing until the voltage collapse happens.

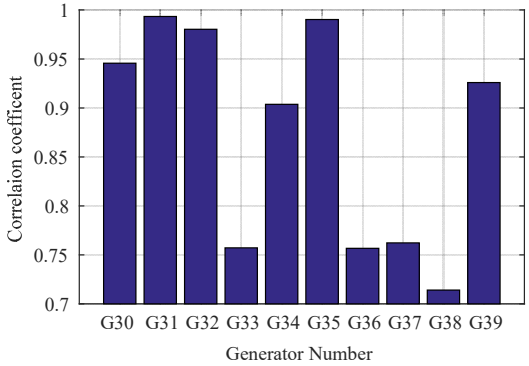

Fig. 13. Correlation coefficients for generator buses and aggregated bus.

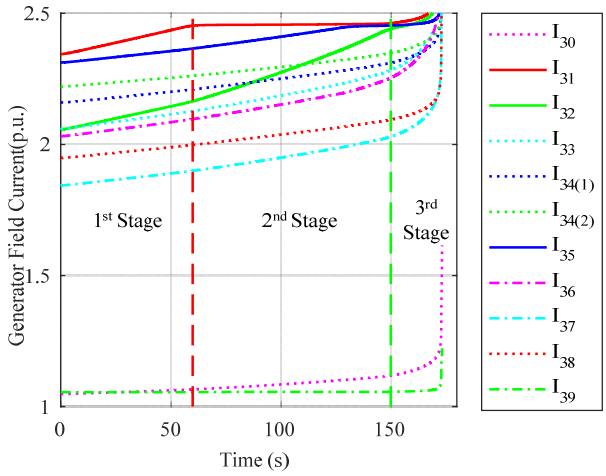

Fig. 14. Generator field currents.

When field current of a generator hits its limit, reactive power output of that generator constricts. Further, if the load continues to increase, reactive power supports from these generators will be significantly reduced, and their terminal voltage will decline. The system may enter voltage instability status even with a small disturbance. As shown in Fig. 15, generators G31, G32 and G35 reach their field current limits, and their reactive power outputs drop significantly since then.

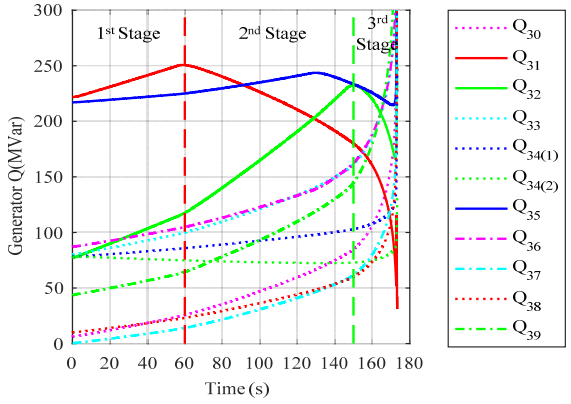

Fig. 15. Generator reactive power outputs.

Fig. 16 shows the results for the active power limit calculation using TE-based method and the proposed method with generator VAR limits considered. The active power limit calculation has been conducted for all measurements, which means that it was calculated 5201 times. The total calculation costs 19.2 seconds, so every calculation takes 0.0037 second. However, it is not necessary to calculate it for all time instant, the configuration can be adjusted according to computation resource and the performance requirement. The active power of Load 8 increases from 522 MW and reaches its limit at 170s, causing voltage collapse. For Stage 1, no generator reaches its over-excitation limit, so the limit predicated by the new method is closed to the TE-based method. When the system enters Stage 2 and Stage 3, the field currents of the generators G31, G32 and G35 approach their limits, and accuracy of the proposed approach become significantly higher than the classical TE approach. The existing approach still gives positive margin when the system collapses at 173s. The active power limit calculated by the proposed approach is reached at the system collapse point.

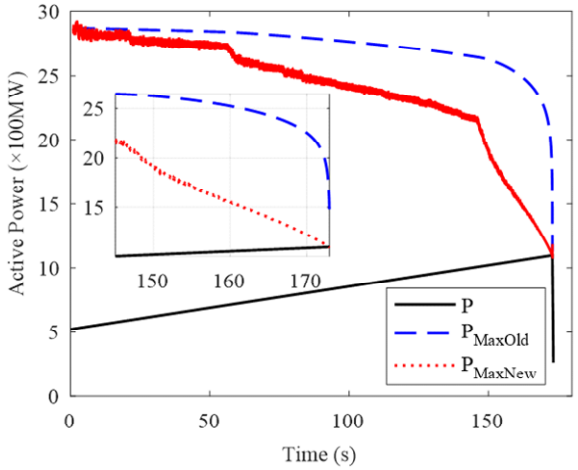

Fig. 16. Pmax comparison.

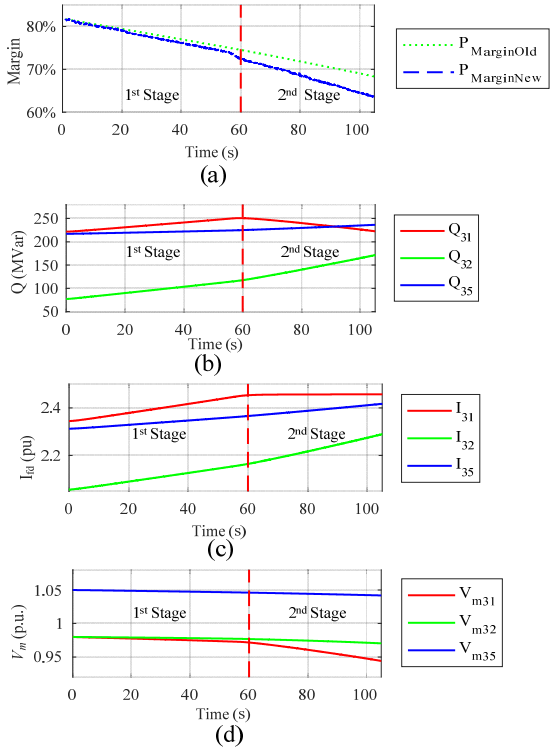

Fig. 17. P margin and field currents.

In Fig. 17(a), an abrupt decline in the *P* margin occurs at

60s as the field current of generator G31 reaches its limit, as shown in Fig. 17(b)-(d). Immediate after that the system enters Stage 2, and the transition reflects the impact from generator G31 with the highest impact factor.

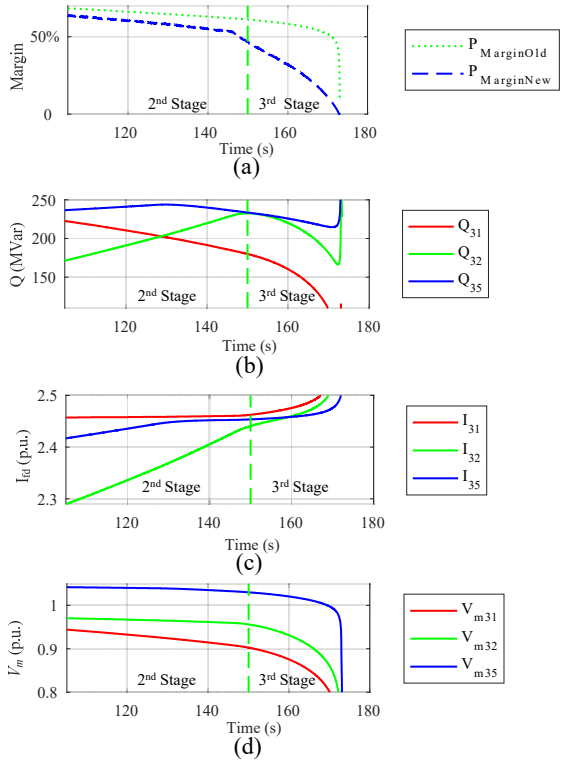

Fig. 18. P margin and field currents.

In Fig. 18, system enters Stage 3 which is triggered by the field current of generator G32 being reached. Similarly, the field current of generator G35 also reaches its limit at 130s, but the impact was limited due to its small impact factor which is less than 0.05. With the quantifiable impact factor, the critical generators are identified correctly and promptly.

Fig. 19 shows improvements in the active power transfer margin calculation using the proposed method. Since no generator hits its Q limit before 60s, the proposed approach and classical TE method give similar margin. After the system enters Stage 2 at 60s, the margin was improved by less than 10% by the proposed method. When the system enters the final stage, as all three generators hit their Q limits, which makes the Q limits a critical factor for the stability margin evaluation. As shown in the figure, the margin calculation improved by the proposed method reaches up to 43%.

Fig. 20 shows the error of the equivalent voltage identified by this method. This error is mainly induced by the linear regression of Eq. (23). It can be observed that, in the 1st and 2nd stages, the error is less than 0.05 p.u. and in all the simulation period except for the critical time of voltage collapse, the error is less than 0.1 p.u.

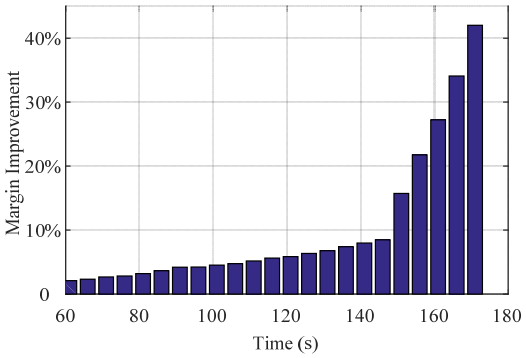

Fig. 19. Pmax comparison.

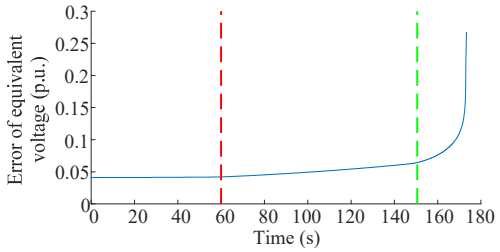

Fig. 20. Error of equivalent voltage ε'.

For industrial applications, PMU measurement errors may exist. In order to analyze the impact of PMU measurement errors on the proposed MBVSA method, two additional study cases with white Gaussian noise on PMU measurements are implemented. Signal to Noise Ratio (SNR) is the metric to quantify the level of noise.

Case A: The SNR is 45dB, which is a reasonable value quantified from comprehensive statistical studies from wide-scale PMUs in different voltage levels [30].

Case B: The SNR is 10dB, which is given for evaluating a worse PMU measurement environment.

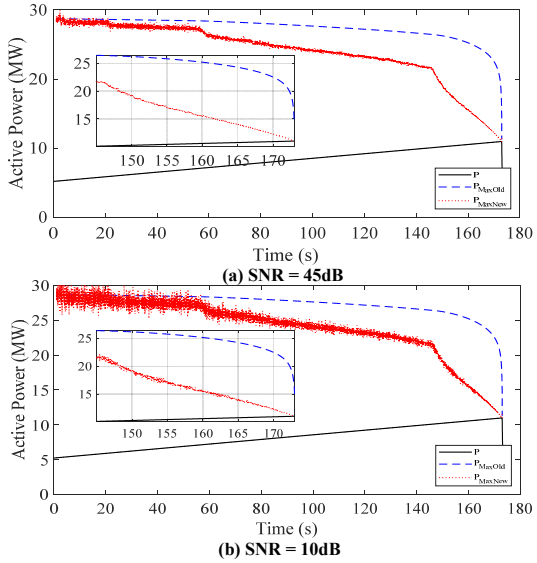

Fig. 21. Comparison with different levels of PMU measurement noise (a) Case A: SNR = 45dB (b) Case B: SNR = 10dB.

Fig. 21 compares the voltage stability margins of Case A and Case B. It can be noticed that the proposed method has

relatively larger noise of stability margin than the traditional method, but the impacts of PMU measurements on the margin are acceptable under reasonable noise level, i.e. SNR = 45dB.

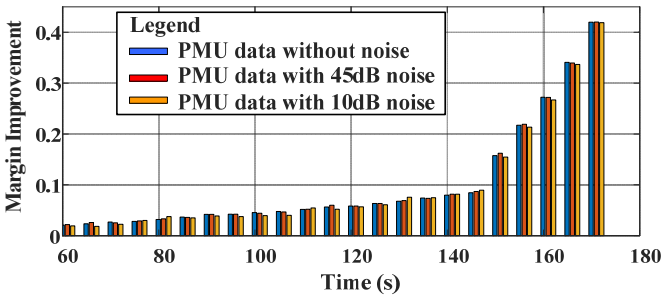

Fig. 22. Comparison of margin Pmax improvement with different levels of PMU measurement noise.

Fig. 22 compares the margin improvement under different levels of noise. It can be observed that the PMU measurement errors on the VSA results can be neglected, if the measurement noise is limited.

V. Conclusion

A measurement-based voltage stability assessment method considering generator VAR limit has been proposed. The proposed approach is capable of predicting both Saddle Node Bifurcation and Limit Induced Bifurcation. The proposed approach gives more accurate system power transfer limits in terms of voltage stability as compared to the existing TE-based method. The proposed method is demonstrated on the two-area system and further validated using the IEEE 39-bus system.

References

[1] P. Zhang, L. Min, and J. Chen, Measurement-based voltage stability monitoring and control, *US Patent 8,126,667*, 2012.

[2] W. Taylor, *Power System Voltage Stability*: McGraw-Hill, 1994.

[3] V. Ajjarapu, and C. Christy, "The continuation power flow: a tool for steady state voltage stability analysis," *IEEE Trans. Power Syst.*, vol. 7, no. 1, pp. 416-423, Feb. 1992.

[4] G. K. Morison, B. Gao, and P. Kundur, "Voltage stability analysis using static and dynamic approaches," *IEEE Trans. Power Syst.*, vol. 8, no. 3, pp. 1159-1171, Aug. 1993.

[5] H.-D. Chiang, A. J. Flueck, K. S. Shah and N. Balu, "CPFLOW: a practical tool for tracing power system steady-state stationary behavior due to load and generation variations," *IEEE Trans. Power Syst.*, vol. 10, no. 2, pp. 623-634, May 1995.

[6] A. Trias, "The holomorphic embedding load flow method," *IEEE PES General Meeting*, San Diego, CA, USA, Jul. 2012.

[7] C. Liu, B. Wang, F. Hu, K. Sun and C. L. Bak, "Online voltage stability assessment for load areas based on holomorphic embedding method," *IEEE Trans. Power Syst.*, vol. 33, no. 4, pp. 3720-3734, Jul. 2018.

[8] B. Wang, C. Liu and K. Sun, "Multi-stage holomorphic embedding method for calculating the power-voltage curve," *IEEE Trans. Power Syst.*, vol. 33, no. 1, pp. 1127-1129, Jan. 2018.

[9] C. Liu, B. Wang, X. Xu, K. Sun, D. Shi and C. L. Bak, "A multidimensional holomorphic embedding method to solve AC power flows," *IEEE Access*, vol. 5, no. 1, 25270-25280, Dec. 2017.

[10] K. Vu, M. M. Begovic, *et al.*, "Use of local measurements to estimate voltage-stability margin," *IEEE Trans. Power Systems*, vol. 14, no. 3, pp. 1029-1035, 1999.

[11] I. Smon, G. Verbic and F. Gubina, "Local voltage-stability index using Tellegen's theorem," *IEEE Trans. Power Syst.*, vol. 21, no. 3, pp. 1267-1275, 2006.

[12] S. Corsi, and G. N. Taranto, "A real-time voltage instability identification algorithm based on local phasor measurements," *IEEE Trans. Power Syst.*, vol. 23, no. 3, pp. 1271-1279, May 2008.

[13] W. Li, T. Chen and W. Xu, "On impedance matching and maximum power transfer," *Electric Power Systems Research*, vol. 80, no. 9, pp. 1082-1088, Sep. 2010.

[14] H. Yuan and F. Li, "A comparative study of measurement-based Thevenin equivalents identification methods," *North America Power Symposium*, 2014.

[15] B. Milosevic and M. Begovic, "Voltage-stability protection and control using a wide-area network of phasor measurements," *IEEE Trans. Power Systems*, vol. 18, no. 1, pp. 121-127, 2003.

[16] I. R. Pordanjani, Y. Wang and W. Xu, "Identification of critical components for voltage stability assessment using channel components transform," *IEEE Trans. Smart Grid*, vol. 4, no. 2, pp. 1122-1132, 2013.

[17] W. Li, Y. Wang and T. Chen "Investigation on the Thevenin equivalent parameters for online estimation of maximum power transfer limits," *IET Gener., Trans. & Distr.*, vol. 4, no. 10, pp. 1180-1187, 2010.

[18] Y. Wang, I. R. Pordanjani *et al.*, "Voltage stability monitoring based on the concept of coupled single-port circuit," *IEEE Trans. Power Syst.*, vol. 26, no. 4, pp. 2154-2163, 2011.

[19] J. H. Liu and C. C. Chu, "Wide-area measurement-based voltage stability indicators by modified coupled single-port models," *IEEE Trans. Power Syst.*, vol. 29, no. 2, pp. 756-764, Mar. 2014.

[20] W. Xu, I. R. Pordanjani *et al.*, "A network decoupling transform for phasor data based voltage stability analysis and monitoring," *IEEE Trans. Smart Grid*, vol. 3, no. 1, pp. 261–270, Mar. 2012.

[21] K. Sun, P. Zhang and L. Min, Measurement-based voltage stability monitoring and control for load centers, *EPRI Report No. 1017798*, 2009.

[22] F. Hu, K. Sun *et al.*, "An adaptive three-bus power system equivalent for estimating voltage stability margin from synchronized phasor measurements," *IEEE PES General Meeting*, 2014.

[23] F. Hu, K. Sun *et al.*, "Measurement-based real-time voltage stability monitoring for load areas," *IEEE Trans. Power Systems*, vol. 31, no. 4, pp. 2787-2798, Jul. 2009.

[24] F. Hu, K. Sun *et al.*, "Measurement-based voltage stability assessment for load areas addressing n-1 contingencies," *IET Gener., Trans. & Distr.*, vol. 11, no. 15, pp. 3731-3738, 2017.

[25] C. A. Canizares, "Voltage stability assessment: concepts, practices and tools," *IEEE/PES Power System Stability Subcommittee special publication* SP101PSS, Aug. 2002.

[26] A. E. Efthymiadis and Y. H. Guo, "Generator reactive power limits and voltage stability," *the 4th International Conferences on Power System Control and Management*, London, pp. 196-199, 1996.

[27] Y. Wang, C. Wang *et al.*, "Incorporating generator equivalent model into voltage stability analysis," *IEEE Trans. Power Systems*, vol. 28, no. 4, pp. 4857-4866, Nov. 2013.

[28] P. Kessel and H. Glavitsch, "Estimating the voltage stability of a power system," *IEEE Trans. Power Del.*, vol. PWRD-1, no. 3, pp. 346-354, Jul. 1986.

[29] P. Kundur, *Power System Stability and Control*, McGraw-Hill, Inc., New York, 1994.

[30] M. Brown, M. Biswal, S. Brahma, S. J. Ranade and H. Cao, "Characterizing and quantifying noise in PMU data" *IEEE PES General Meeting*, Boston, MA, USA, Jul. 2016.

Chengxi Liu (S'10-M'13-SM'18) received the B.S. and M.S. degrees in electrical engineering from Huazhong University of Science and Technology, China, in 2005 and 2007, respectively, and the Ph.D. degree from Aalborg University, Denmark, in 2013. He was with Energinet.dk, the Danish TSO until 2016 and Research Associate, the University of Tennessee, USA until 2018. He was an Associate Professor with the Department of Energy Technology, Aalborg University. He is currently a Professor with the School of Electrical Engineering and Automation, Wuhan University. His research interests include stability and control of power systems, simulation methods of power systems, big data and artificial intelligence applied in power systems.

Fengkai Hu received the B.S. and M.S. degrees from the University of Electronic Science and Technology of China, and Ph.D. degree in Electrical Engineering from the University of Tennessee, Knoxville. His research interests include power system stability and control, wide area measurement system, energy market and microgrid.

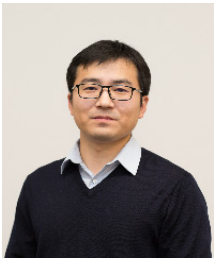

Di Shi (M'12-SM'17) received his Ph.D. degree in electrical engineering from Arizona State University. He is the Department Head of the AI & System Analytics Group at GEIRI North America (GEIRINA), San Jose, CA, USA. Prior to joining GEIRINA, Dr. Shi was a Research Staff Member at NEC Laboratories America. His research interests include PMU data analytics, AI, Energy storage systems, IoT for power systems, and renewable integration. He is editor of IEEE Transactions on Smart Grid and IEEE Power Engineering Letters.

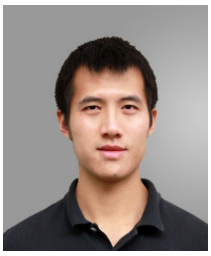

Xiaohu Zhang (S'12-M'17) received the B.S. degree in electrical engineering from Huazhong University of Science and Technology, Wuhan, China, in 2009, the M.S. degree in electrical engineering from Royal Institute of Technology, Stockholm, Sweden, in 2011, and the Ph.D. degree in electrical engineering at The University of Tennessee, Knoxville, in 2017. Currently, he works as a power system engineer at GEIRI North America, San Jose, CA, USA. His research interests are power system operation, planning and stability analysis.

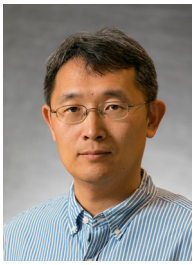

Kai Sun (M'06–SM'13) received the B.S. degree in automation in 1999 and the Ph.D. degree in control science and engineering in 2004 both from Tsinghua University, Beijing, China. He is an associate professor at the Department of EECS, University of Tennessee, Knoxville, USA. He was a project manager in grid operations and planning at the EPRI, Palo Alto, CA from 2007 to 2012. Dr. Sun serves in the editorial boards of IEEE Transactions on Power Systems, IEEE Transactions on Smart Grid and IEEE Access.

Zhiwei Wang (M'16-SM'18) received the B.S. and M.S. degrees in electrical engineering from Southeast University, Nanjing, China, in 1988 and 1991, respectively. He is the President of GEIRI North America, San Jose, CA, USA. Prior to this assignment, he served as President of State Grid US Representative Office, New York City, from 2013 to 2015, and President of State Grid Wuxi Electric Power Supply Company from 2012 to 2013. His research interests include power system operation and control, relay protection, power system planning, and wide-area measurement systems.